



Adsorption of basic red 9 onto activated carbon derived from immature cotton seeds: isotherm studies and error analysis

N. Sivarajasekar, R. Baskar*

Department of Chemical Engineering, Kongu Engineering College, Perundurai, Erode 638052, Tamil Nadu, India
Tel. +91 4294 226602; Fax: +91 4294 220087; email: naturebaskar@yahoo.co.in

Received 18 April 2013; Accepted 1 August 2013

ABSTRACT

The activated carbon produced from immature cotton seeds via sulphuric acid activation was utilized for adsorption of the basic red 9 from the aqueous solution. Adsorbent possessed a larger surface area ($495.96 \text{ m}^2/\text{g}$), methylene blue number (42) and iodine number (510). The process parameters of the sorption system, such as pH of the solution (2–12), temperature ($20\text{--}40^\circ\text{C}$) agitation time (1–5 h) and initial BR9 concentration (50–250 mg/l), were studied to understand their effects on BR9 removal. The optimized parameters are found to be pH: 12, temperature: 40°C , agitation time: 3 h and initial concentration: 150 mg/l. The experimental equilibrium data were analysed using a single-parameter model (Henry's law), six two-parameter models (Langmuir, Freundlich, Temkin, Dubinin–Radushkevich, Smith, and Javanovic), eleven three-parameter models (Redlich–Peterson, Sips, Toth, Hill, Khan, Brunauer–Emmett–Teller (BET), Fritz–Schlunder-III, Vieth–Sladek, Radke–Prausnitz, Brouers–Sotolongo, and Unilin), five four-parameter models (Baudu, Parker, Marczewski–Jaroniec, Fritz–Schlunder-IV and Weber–van Vliet) and a five-parameter model (Fritz–Schlunder-V). Non-linear regression analysis was employed to identify the best-fit isotherm based on the error functions: sum of the square error, derivative of hybrid fractional error function, derivative of Marquardt's percentage standard deviation, average relative error, the sum of absolute errors and statistical comparison values: coefficient of determination (R^2), root-mean-square error (RMSE) and non-linear chi-square test (χ^2). Among the all adsorption isotherms considered, Fritz–Schlunder-V was found to be a perfect representation of the experimental equilibrium data (R^2 : 0.9998081, RMSE: 0.1018119, χ^2 : 0.0023423). The goodness of the models to explain the equilibrium data was in the order: Fritz–Schlunder-V > Fritz–Schlunder-IV > Brouers–Sotolongo > Unilin > Marczewski–Jaroniec > Baudu > Sips > Hill > Vieth–Sladek > Fritz–Schlunder-III > Redlich–Peterson > Khan > Radke–Prausnitz > BET > Weber–van Vliet > Langmuir > Parker > Jovanovic > Freundlich.

Keywords: Adsorption; Basic red 9; Isotherms; Error analysis; Non-linear regression; Activated carbon

1. Introduction

Industries such as textile, plastic, tannery, packed food, pulp and paper, paint and electroplating are

extensively using more than 10,000 synthetic dyes in their processes [1–3]. Coloured effluents released from these industries worsen the aesthetic value of the water bodies and adversely affects the photosynthesis of aquatic plants by hindering the penetration of light.

*Corresponding author.

Among the variety of dyes used, cationic dyes are widely employed in acrylic, wool, nylon and silk dyeing. Complete biodegradation of these dyes are very difficult due to their complex chemical structure having substituted aromatic groups [4–7]. These dyes may also decompose into carcinogenic aromatic amines under anaerobic conditions, so discharge of these dye bearing effluents into water bodies can cause harmful effects such as allergic dermatitis, skin irritation, mutations and cancer [4–7]. As such discharges are increasing year by year, eco-system as a whole is in great threat and, therefore, there is an urgent need to develop effective methods for removal of dyes via physical, chemical and biological methods including sorption, coagulation, precipitation, ion-exchange, electrochemical, membrane filtration, advanced oxidation and biodegradation which have been tried by many researchers. Among all the methods mentioned, adsorption is an effective and eco-friendly process for colour removal from wastewaters due to its simple design, easy operation and its efficacy for a wide range of compounds [4,5,7]. Activated carbon has been extensively utilized as adsorbent in the recent past due to the presence of various oxygenated functional surface groups and its pore structure. Recognizing the high cost of activated carbon, many investigators have attempted for replacing it by cheap, commercially available and renewable bio-based materials [5,8,9]. Some among them include: apricot stones [10], *Arundo donax* [11], white oak [12], olive mill waste [13], lignin [14], coir pith [15], corn cob [16], rice husk [17], walnut shell [18], date pits [19], palm shell [20], coffee bean husk [21], coconut shell [22], peanut hull [23], sewage sludge [24], etc.

Our search for new precursor for activated carbon came to an end when we located immature cotton seeds—a reject from seed manufacturers. As per the current scenario, 85% of the world cotton production is shared by 10 countries, namely China, the USA, India, Pakistan, Uzbekistan, Brazil, Turkey, Australia, Greece and Syria. Among them, India is the third largest country which produced $5,787 \times 10^3$ metric tonnes of un-ginned cotton in the 2011/2012 market year [25]. Generally, cotton seeds are separated from lint in the ginning operation and further processed to extract cotton seed oil. The immature cotton seeds unfit for germination and having poor oil content are usually discarded as waste and needs only activation to transform them into cheap and quality adsorbent. Even though many agricultural and waste materials were used as adsorbents for the removal of colour, adsorbent derived from immature cotton seeds were never reported yet to the best of our knowledge. Therefore, an attempt was made to prepare adsorbent

from immature cotton seeds via chemical activation and to examine its ability of up-taking basic red 9 (BR9) from aqueous solution. The effect of significant process parameters (initial dye concentration, contact time, initial pH and temperature) on the rate of BR9 adsorption was also evaluated.

An accurate mathematical description of equilibrium adsorption capacity i.e. the most suitable correlation for the equilibrium curve is vital for reliable prediction of adsorption parameters and quantitative comparison of adsorption behaviour for an adsorbent–adsorbate system in order to optimize the design and to understand the adsorption mechanism [26–28]. Even though there are quite a few isotherm models available for analysing experimental data and describing the equilibrium of adsorption, there is no general procedure offered to identify a best-fitting isotherm [26–29]. To determine isotherm constants for single component adsorption isotherms, currently two methods are available such as non-linear regression analysis and linear regression analysis [26,27,29]. Recently, numerous studies have presented that the linearization of a non-linear isotherm expression produces different results, in such cases non-linear regression analysis is the only option [30–33]. In the case of non-linear regression, the selection of error functions showed a change in the values of individual isotherm constants [30,33]. This could be efficiently pacified by selecting an optimization procedure such as sum of normalized errors [29,30]. Therefore, the equilibrium data resulting from batch adsorption experiments were analysed by using 24 different types of isotherm models and a best fit among them was investigated by comparing sum of normalized errors and statistical comparison values. Such a study will be significantly useful in understanding sorption mechanism for theoretical evaluation, designing and assessing the performance of sorption systems.

2. Material and methods

2.1. Chemicals

Basic red 9 (Molecular weight: 387.28 g/mol) was obtained from Hi media laboratories Ltd, Mumbai. All other chemicals used in this research were obtained from Merck India Ltd, Mumbai. The structure of BR9 is shown in Fig. 1.

2.2. Preparation of dye solution

The stock solution of BR9 was prepared by dissolving weighed amount of dye in 1 l of doubly distilled water. All working solutions were prepared

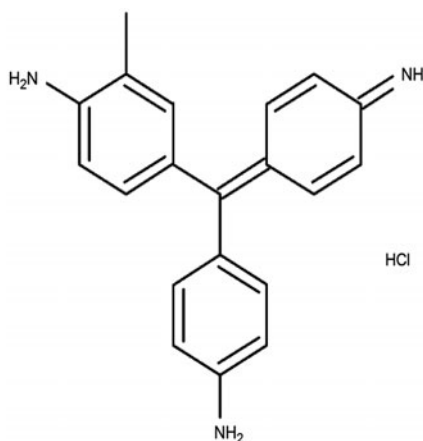


Fig. 1. Structure of BR9 dye molecule.

by diluting the stock solution with doubly distilled water to the desirable concentration. The initial pH of each solution was adjusted to the required value by adding 0.1N HCl or 0.1N NaOH solutions before mixing the adsorbent with the dye solution. The concentration of dye in the sample was analysed using a double beam UV–Vis spectrophotometer (ELICO-SL244, India) at a maximum wavelength of 550 nm.

2.3. Activated carbon preparation

Immature cotton seeds were collected from cotton seed producers near Attur, Tamil Nadu, India. The collected seeds were washed thoroughly with distilled water to remove dirt and dried at 40°C in a temperature-controlled oven for three days. The dried biomass was soaked with 98% concentrated sulphuric acid in the weight ratio of 1:4. In order to achieve effective activation, the acid-soaked biomass was stirred periodically and kept for 12 h. The resultant slurry was carefully washed with doubly distilled water. Further, the traces of acid were removed by washing the material twice with 0.1N sodium bicarbonate solution. The resultant material immature cotton seed-activated carbon (ICSAC) was sundried and finely ground to the required size, stored in an air tight container and subsequently used in the batch adsorption experiments. The characteristics of ICSAC are given in Table 1.

2.4. Batch adsorption

Batch adsorption studies were carried out by agitating known amount of adsorbent with 200 ml of dye solution taken in Erlenmeyer flasks and agitating them using a thermo-regulated shaker (GeNei SLM-IN-OS-16, India) operating at 100 rpm. The standard experimental conditions for the batch adsorption

experiments are given in Table 2. The samples were withdrawn from the flasks at predetermined time intervals for studying effect of parameters and at equilibrium time for isotherm studies. Obtained samples were centrifuged at 8,000 rpm for 2 min (Remi R-24 Centrifuge, India) to remove the suspended solids. The clear supernatants were analysed for the residual dye concentration using double beam UV–Vis spectrophotometer (ELICO-SL244, India). Percentage of dye removal from bulk dye solution was calculated using the following equation:

$$\% R = \frac{C_i - C_0}{C_i} \times 100 \quad (1)$$

where C_i and C_0 (mg/l) are initial and final concentration of the dye in the aqueous solution. The equilibrium adsorption capacity was calculated as

Table 1
Characteristics of ICSAC

Parameter	Values
pH	6.5
Bulk density (g/ml)	0.52
Particle diameter (mm)	0.088
Methylene blue number (mg/g)	42
Iodine number (mg/g)	510
BET surface area (m ² /g)	496.5

Table 2
Different process conditions used for adsorption of BR9 onto ICSAC

Process parameters	Range of study	Other conditions
Initial pH	2, 7 and 12	Contact time: 3 h; initial dye concentration: 150 mg/l; temperature: 30°C; adsorbent dose: 5 mg/l
Temperature	20, 30 and 40°C	Contact time: 3 h; initial dye concentration: 150 mg/l; adsorbent dose: 5 mg/l; initial pH: 12
Agitation time	1, 2, 3, 4 and 5 h	Temperature: 40°C; pH: 12; different dye concentrations: 50, 100 and 150 mg/l
Initial BR9 concentration	50, 100, 150, 200 and 250 mg/l	Temperature: 40°C; pH: 12; contact time: 5 h; adsorbent dose: 5 mg/l

$$q_e = C_0 - C_e \times \frac{V}{M} \quad (2)$$

where C_e (mg/l) is equilibrium concentration, V (l) is volume of dye solution taken for batch experiment and M (g) is the weight of ICSAC.

As reported elsewhere [34–37], optimum values of the parameters were determined based on the experimental order (solution pH, temperature, initial solute concentration and contact time). Further, it is also verified that the change in experimental order did not alter the optimum values.

2.5. Theory

2.5.1. Isotherm studies

During the adsorption process, dynamic equilibrium is established between the dye molecules in the aqueous phase and the adsorbent surface at isothermal conditions which is expressed by the isotherms. Optimum loading of adsorbents can be easily estimated from these adsorption isotherms [38]. Better insight of the adsorbent–adsorbate binding can be explained by the most fitted isotherms that depend on the nature of the sorption system. Several models were proposed for describing adsorption equilibrium.

2.5.1.1. Single-parameter model. Henry's law. Henry's law [39] is a well fit to the adsorption of solutes on a uniform surface of adsorbent at sufficiently low concentrations such that all solute molecules are isolated from their nearest neighbours. According to this isotherm, the fluid phase and adsorbed phase equilibrium concentrations can be related in a linear equation:

$$q_e = HC_e \quad (3)$$

where q_e (mg/g) is the amount of dye adsorbed on the adsorbent surface at equilibrium and H (l/mg) is adsorption equilibrium constant known as Henry constant. The higher value of H indicates a stronger interaction between the adsorbent and the solute molecules [40].

2.5.1.2. Two-parameter models. Langmuir isotherm. According to the Langmuir isotherm, the monolayer adsorption is taking place on a structurally homogeneous adsorbent where all the adsorption sites are identical and energetically equivalent (i.e. constant heat of adsorption for all sites) [41]. As the intermolecular forces decrease rapidly with distance, the existence of monolayer coverage of the dye at the outer surface of the adsorbent can be predicted using this isotherm model [42]. This model reduces to linear

Henry's law at low solute concentrations and at high solute concentrations; it predicts a constant monolayer adsorption capacity. Langmuir Isotherm can be written as

$$q_e = \frac{q_{mL} b_L C_e}{1 + b_L C_e} \quad (4)$$

where $q_{mL} = K_L/b_L$ (mg/g) is the maximum monolayer adsorption capacity predicted by Langmuir isotherm, K_L (l/g) and b_L (l/mg) are the Langmuir model constants. Weber and Chakravorti [43] proposed a separation factor (R_L) to understand the favourability of isotherm, which is defined as

$$R_L = \frac{1}{1 + C_0 b_L} \quad (5)$$

Langmuir isotherm could be utilized for the estimation of the surface areas of porous solids as the substitute for Brunauer–Emmett–Teller (BET) method [44–46]. By considering that the adsorbent surface is homogenous and entirely covered by dye molecules, BET isotherm model could be reduced to the Langmuir isotherm [47]. Therefore, based on the maximum monolayer adsorption capacity (q_m) calculated with the Langmuir equation and the projected area of an dye molecule A (nm²), the specific surface area S_{sp} (m²/g) of the ICSAC can be calculated using the following equation:

$$S_{sp} = \frac{6.023 \times 10^{23} \times A \times q_m}{1,000} \quad (6)$$

Freundlich isotherm. The empirical Freundlich isotherm model describes the non-ideal and reversible nature of adsorption, not restricted to the formation of monolayer such as Langmuir isotherm. Thus, multi-layer adsorption, with non-uniform distribution of adsorption heat and affinities over the heterogeneous surface, can be explained by its relationship [48]:

$$q_e = K_F C_e^{1/n_F} \quad (7)$$

where K_F (l/g) is the Freundlich isotherm constant and n_F is Freundlich exponent. The magnitude of $1/n_F$ ranges between 0 and 1 is a degree of adsorption intensity or surface heterogeneity; a value below unity indicates chemisorption process where as above one implies cooperative adsorption [49].

Temkin Isotherm. The isotherm postulated by Temkin and Pyzhev [50] relates the effects of heat of

adsorption that decreases linearly with the coverage of the solute and the adsorbent interactions on the surface at moderate values of solute concentrations. This isotherm assumes that the adsorption is characterized by a uniform distribution of binding energies up to some maximum energy. It can be represented as

$$q_e = \frac{RT}{b_T} \{\ln(a_T C_e)\} \quad (8)$$

where b_T (J/mol) is the Temkin isotherm constant related to heat of sorption, a_T (1/g) is the Temkin isotherm constant, R is the gas constant (8.314 J/molK) and T (K) is the absolute temperature.

Dubinin–Radushkevich isotherm. Dubinin proposed a well-known equation for the analysis of isotherms of a high degree of regularity [51,52]. This isotherm states that the characteristic sorption curve is associated to the porous structure of the adsorbent. It facilitates to find the value of mean free energy of adsorption per mole of solute as it is transferred from the solution to the solid surface. The expression of the Dubinin–Radushkevich isotherm equation is:

$$q_e = q_{mDR} \exp\left\{-K_{DR} \left[RT \ln\left(1 + \frac{1}{C_e}\right)\right]^2\right\} \quad (9)$$

where q_{mDR} (mg/g) is the maximum monolayer adsorption capacity predicted by Dubinin–Radushkevich isotherm, ε (mol²/KJ²) is Polanyi potential and the K_{DR} is Dubinin–Radushkevich constant. The mean free energy (E) can be computed using the following relationship [53]:

$$E = \frac{1}{\sqrt{2K_{DR}}} \quad (10)$$

The magnitude of E (kJ/mol) is useful for estimating the type of sorption reaction. If the values of E is around 8–16 kJ/mol, means that the adsorption is nothing but ion-exchange reaction.

Smith isotherm. The Isotherm proposed by Smith [54] takes into account the progressive enlargement of the adsorptive surface which must inevitably result in an increase in the number of adsorptive sites exposed within the structure that accompanies swelling in an aqueous environment. During the desorption process, the solute molecules bound to rigid structural elements of appreciably superior dimensions get involved to block the collapse of the structure. The Smith isotherm can be written as

$$q_e = W_{s1} - W_{s2} \ln(1 - C_e) \quad (11)$$

where W_{s1} and W_{s2} are Smith isotherm constants.

Jovanovic isotherm. Jovanovic [55] developed a model keeping the same assumptions as that of Langmuir isotherm and also considered the surface binding vibrations of the adsorbed species. The Jovanovic isotherm represents another approximation for monolayer localized adsorption without lateral interactions. It reduces to the Langmuir isotherm at high concentrations but does not obey the Henry’s law. According to this isotherm, the energy distribution for Jovanovic local behaviour is a quasi-Gaussian function skewed in the path of high adsorption energies. The Jovanovic equation is:

$$q_e = q_{mj}(1 - e^{K_j C_e}) \quad (12)$$

K_j is the Jovanovic isotherm constant related to the free energy of adsorption and q_{mj} (mg/g) is the maximum monolayer adsorption capacity from this model.

2.5.1.3. Three-parameter models. *Redlich–Peterson isotherm.* Redlich and Peterson [56] included the characteristics of both Langmuir and Freundlich isotherms into a single equation which incorporates three parameters into an empirical equation. It has a linear dependence on concentration in the numerator and an exponential function in the denominator [57] to represent adsorption equilibrium over a wide range of concentrations. This isotherm approaches Freundlich isotherm model at high concentration and approaches Henry’s law at low concentration. It has the following form:

$$q_e = \frac{K_{RP1} C_e}{1 + K_{RP2} C_e^{\beta_{RP}}} \quad (13)$$

where K_{RP1} (1/g) and K_{RP2} (1/mg) are the Redlich–Peterson isotherm constants, and β_{RP} is the Redlich–Peterson model exponent. While β_{RP} value tends to zero this isotherm approaches Freundlich isotherm and β_{RP} value tends to unity this isotherm approaches Langmuir isotherm.

Sips isotherm. Sips [58] proposed a combined form of Langmuir and Freundlich isotherms deduced for predicting the heterogeneous adsorption systems. This model overcomes the disadvantage of the increasing solute concentration linked with Freundlich isotherm. At low solute concentrations, it effectively reduces to Freundlich isotherm and does not obey Henry’s law

whereas at high solute concentrations, it predicts a monolayer sorption capacity characteristic of the Langmuir isotherm. Sips isotherm is given by

$$q_e = \frac{K_s q_{mS} C_e^{\frac{1}{n_s}}}{1 + K_s C_e^{\frac{1}{n_s}}} \quad (14)$$

where K_S (l/g) is the Sips isotherm constant, q_{mS} (mg/g) is the maximum monolayer adsorption capacity by Sips isotherm and n_S is the Sips model exponent.

Toth isotherm. An empirical equation developed from potential theory by Toth [59] for improving the outcomes of Langmuir isotherm found useful in describing heterogeneous adsorption systems which assumes that the majority of the active sites have adsorption energy lower than the maximum or mean value. Toth isotherm in the form of asymmetrical quasi-Gaussian energy distribution is

$$q_e = \frac{q_{mT} C_e}{(K_T + C_e^{n_T})^{1/n_T}} \quad (15)$$

where q_{mT} (mg/g) is the maximum monolayer adsorption capacity predicted by Toth isotherm, K_T is the Toth isotherm constant and n_T is the Toth isotherm exponent. n_T is a scale of surface heterogeneity. If n_T approaches unity, this suggests that the process occurs on a homogenous surface.

Hill isotherm. Hill [60] postulated an isotherm from the non-ideal competitive adsorption [61] model to describe the binding of different solutes onto a homogeneous adsorbent. The model assumes that adsorption is a cooperative occurrence, owing to the ligand binding ability at one site on the macromolecule, which tends to influence different binding sites on the same macromolecule. The Hill equation is:

$$q_e = \frac{q_{mH} C_e^{n_H}}{K_H + C_e^{n_H}} \quad (16)$$

where q_{mH} (mg/g) is the maximum monolayer adsorption capacity given by Hill isotherm, K_H is the Hill isotherm Constant and n_H is Hill cooperativity coefficient. If $n_H > 1$, positive cooperativity in binding, $n_H = 1$, non-cooperative or hyperbolic binding, and $n_H < 1$, negative cooperativity in binding.

Khan isotherm. Khan et al. [62] has suggested a generalized equation for bi-solute adsorption from dilute aqueous solutions. This isotherm has a distinctive characteristic such as covering both extremes Langmuir on one and Freundlich isotherm on the other

hand. The generalized model for a single solute Khan isotherm could be in the form of the simple expression:

$$q_e = \frac{q_{mK} b_K C_e}{(1 + b_K C_e)^{a_K}} \quad (17)$$

where q_{mK} (mg/g) is the maximum monolayer adsorption capacity predicted by Khan isotherm, b_K is Khan isotherm constant and a_K is Khan isotherm exponent. When a_K is equal to unity, above equation reduces to the Langmuir isotherm and at large values of C_e reduces to the Freundlich isotherm.

BET isotherm. The BET equation is a special form of Langmuir Isotherm often used to describe the adsorption of a gas on a solid surface at equilibrium [63]. This model incorporates multilayer adsorption without omitting the assumptions of Langmuir isotherm and illustrates the adsorption phenomena onto a homogeneous surface after the successful formation of a monolayer. This isotherm fits well for physi-sorption for non-micro porous adsorbent surfaces. The BET isotherm equation is

$$q_e = \frac{q_{mBET} \alpha_{BET} C_e}{(1 - \beta_{BET} C_e)(1 - \beta_{BET} C_e + \alpha_{BET} C_e)} \quad (18)$$

where q_{mBET} (mg/g) is the maximum monolayer adsorption capacity predicted by BET isotherm, and α_{BET} and β_{BET} are BET isotherm constants.

Vieth–Sladek isotherm. Vieth–Sladek [64] developed a model during the path of formulating a new technique for estimating diffusion rates in solid adsorbents from transient adsorption. This isotherm has the distinctive two portions: one described by a linear portion (Henry's law) and remaining commonly observed non-linear portion (Langmuir isotherm). The linear portion explains the physi-sorption of gas molecules over the amorphous surfaces of adsorbent and the non-linear portion illustrates the adherence of gas molecules to sites on the porous surfaces of adsorbent. The Vieth–Sladek isotherm can be written as

$$q_e = \frac{q_{mVS} b_{VS} C_e}{(1 + b_{VS} C_e)^{n_{VS}}} \quad (19)$$

where q_{mVS} (mg/g) is the maximum monolayer adsorption capacity given by Vieth–Sladek isotherm, b_{VS} is the Vieth–Sladek equilibrium constant and n_{VS} is the Vieth–Sladek model exponent.

Radke–Prausnitz isotherm. A simple equation presented by Radke and Prausnitz [65,66] based on thermodynamic ideal solution concepts for dilute solutions found useful for heterogeneous equilibrium studies. This isotherm proposed a slight modification to the Langmuir equation by introducing a coefficient to improve the fit to the experimental data. At low concentrations, the isotherm reduces to Henry’s law, nevertheless at high concentration the equilibrium adsorption capacity tends to infinity similar to the Freundlich equation. The Radke–Prausnitz isotherm model is depicted as

$$q_e = \frac{q_{mRP}K_{RP}C_e}{(1 + q_{mRP}C_e)^{n_{RP}}} \quad (20)$$

where q_{mRP} (mg/g) is the maximum monolayer adsorption capacity predicted by Radke–Prausnitz isotherm, K_{RP} is the Radke–Prausnitz equilibrium constant and n_{RP} is the Radke–Prausnitz model exponent.

Brouers–Sotolongo isotherm. A model in the form of deformed exponential (Weibull) function known as Brouers and Sotolongo isotherm [67] is given by

$$q_e = q_{mBS}(-K_{BS}C_e^{n_{BS}}) \quad (21)$$

where q_{mBS} (mg/g) is the maximum monolayer adsorption capacity predicted by Brouers–Sotolongo isotherm, K_{BS} is the Brouers–Sotolongo equilibrium constant and n_{BS} is the Brouers–Sotolongo model exponent. One of the useful findings from this model is that the sorption energy distribution and the energy heterogeneity of the adsorbent surface can be measured from model exponent n_{BS} at the given temperature.

Fritz–Schlunder-III isotherm. An empirical expression suggested by Fritz and Schlunder [68] can fit a wide range of experimental data due to large number of coefficients in their isotherm. Fritz–Schlunder isotherm-III has the following form:

$$q_e = \frac{q_{mFS}K_{FS}C_e}{1 + q_{mFS}C_e^{n_{FS}}} \quad (22)$$

where q_{mFS} (mg/g) is the maximum monolayer adsorption capacity predicted by Fritz–Schlunder-III isotherm, K_{FS} is the Fritz–Schlunder-III equilibrium constant and n_{FS} is the Fritz–Schlunder-III model exponent.

Unilin isotherm. There is another one empirical correlation developed by Valenzuela and Myers which

was suggested for the equilibrium data analysis by Unilin [69]. This isotherm is represented as:

$$q_e = \frac{q_{mU}}{2b_U} \ln \left(\frac{a_U + C_e e^{b_U}}{a_U + C_e e^{-b_U}} \right) \quad (23)$$

where q_{mU} (mg/g) is the maximum monolayer adsorption capacity predicted by Unilin isotherm, a_U is the Unilin equilibrium constant and b_U is the Unilin model exponent.

2.5.1.4. Four-parameter models. Baudu isotherm. Baudu [70] has estimated the Langmuir coefficients, b and q_{mL} , by the measurement of tangents at different equilibrium concentrations and he came to a conclusion that they are not constants in a broad concentration range. So, he transformed the Langmuir equation to the following expression:

$$q_e = \frac{q_{mB}b_B C_e^{(1+x+y)}}{1 + b_B C_e^{(1+x)}} \quad (24)$$

which is only valid to the range of $(1+x+y) < 1$ and $(1+x) < 1$. Where q_{mB} (mg/g) is the maximum monolayer adsorption capacity predicted by Baudu isotherm, b_B is the Baudu equilibrium constant, and x and y are the Baudu model exponents.

Parker isotherm. A four-parameter non-linear isotherm was discussed by Parker [71] in his studies. He derived an exponential form of isotherm from the Freundlich equation by introducing few modifications. The Parker Isotherm can be written as

$$q_e = q_{mP} \left[-a_P \left(RT \ln \frac{C_s}{C_e} \right)^{b_P} \right] \quad (25)$$

where C_s (mg/l) is the concentration required for full surface coverage, q_{mP} (mg/g) is the maximum monolayer adsorption capacity predicted by Parker isotherm, a_P is the Parker equilibrium constant and b_P is the Parker model exponent.

Marczewski–Jaroniec Isotherm. Marczewski–Jaroniec isotherm [71] which is also known as the four-parameter generalized Langmuir equation is proposed based on the assumptions of Langmuir isotherm and the distribution of adsorption energies in the active sites. This isotherm is given as

$$q_e = q_{mMJ} \left(\frac{(K_{MJ}C_e)^{n_{MJ}}}{1 + (K_{MJ}C_e)^{n_{MJ}}} \right)^{\frac{m_{MJ}}{n_{MJ}}} \quad (26)$$

where q_{mMJ} (mg/g) is the maximum monolayer adsorption capacity predicted by Marczewski–Jaroniec isotherm, K_{MJ} is the Marczewski–Jaroniec equilibrium constant, and n_{MJ} and m_{MJ} are the Marczewski–Jaroniec model exponents.

Fritz–Schlunder-IV isotherm. Another four-parameter model of Langmuir–Freundlich type was developed empirically by Fritz and Schlunder [68]. It is expressed by the equation:

$$q_e = \frac{A_{FS}C_e^{a_{FS}}}{1 + B_{FS}C_e^{b_{FS}}} \quad (27)$$

where A_{FS} and B_{FS} are the Fritz–Schlunder-IV equilibrium constants, and a_{FS} and b_{FS} are the Fritz–Schlunder-IV model exponents. These exponents' values are bound to be less than or equal to one. At high aqueous phase concentrations of solute, Fritz–Schlunder-IV isotherm reduces to Freundlich equation. On the other hand for $a_{FS}=b_{FS}=1$, this isotherm reduces to Langmuir isotherm.

Weber–van Vliet isotherm. Weber and van Vliet [72] have stated an empirical relation with four parameters to illustrate the heterogeneous equilibrium adsorption data. It is given as:

$$C_e = P_1 q_e^{(P_2 q_e^{P_3} + P_4)} \quad (28)$$

where P_1 , P_2 , P_3 and P_4 are Weber–van Vliet model parameters.

2.5.1.5. Five-parameter models. Fritz–Schlunder-V isotherm. Fritz and Schlunder [68] have proposed a five-parameter empirical expression which could be applied to a wide range of equilibrium data that can be written in the following form:

$$q_e = \frac{q_{mFS5} K_1 C_e^{\alpha_{FS}}}{1 + K_2 C_e^{\beta_{FS}}} \quad (29)$$

where q_{mFS5} (mg/g) is the maximum monolayer adsorption capacity predicted by Fritz–Schlunder-V isotherm, K_1 and K_2 are the Fritz–Schlunder-V equilibrium constants, and α_{FS} and β_{FS} are the Fritz–Schlunder-V model exponents. This isotherm is valid only in the range of $\alpha_{FS} \leq 1$ and $\beta_{FS} \leq 1$.

2.5.2. Non-linear regression analysis

Usually, by linear regression magnitude of the coefficient of determination, (R^2) is taken as the index

for the quality of the fit to the experimental adsorption data. However, transformation of non-linear equations into linear ones utterly upset their error structure and may also defy the error variance of normality assumptions of standard least squares [73,74]. Additionally, linear regression is not always a good choice to apply for isotherms with more than two parameters and, therefore, the non-linear regression analysis is preferable to determine isotherm parameters [75–77]. Generally, the optimization procedure required an error function to be able to evaluate the fit of the equation to the experimental data and the isotherm parameters derived can be affected by the choice of the error function [28,78,79]. Various error functions that can be employed are: sum of the square error (ERRSQ), derivative of hybrid fractional error function (HYBRID), derivative of Marquardt's percentage standard deviation (MPSD), average relative error (ARE) and the sum of absolute errors (EABS). The statistical comparison values such as coefficient of determination (R^2), root-mean-square error (RMSE) and non-linear chi-square test (χ^2) can also be used to gauge the goodness of the fit. More detailed definitions of the error functions and statistical comparison values are presented in Table 3. These error functions and statistical comparison values can be evaluated using the tools like *solver* add-in with Microsoft's spread sheet, Excel (Microsoft, 1995) through any of the iteration methods. The application of these five different error methods will produce different isotherm parameter sets; therefore, it is hard to directly recognize an overall optimum parameter set. In order to facilitate a meaningful comparison between the isotherm parameter sets, the procedure of "sum of the normalized errors" (SNE) is usually adopted [28,29,66]. This approach allows a direct comparison of the scaled errors and thus identifies the isotherm parameter that would provide the closest fit to the measured data. The parameter set derived based on the smallest SNE will be an optimal one providing that there is no bias in the data sampling and type of error functions selected.

3. Result and discussion

3.1. Effect of pH

As pH is an important monitoring parameter in the adsorption process to achieve a maximum dye removal by an adsorbent, the effect of pH has been studied by varying the same in the range of 2–12 (Fig. 2). The extent of dye sorption onto ICSAC showed an increase (69.52–92.12%) as the pH increased from 2 to 12 and the highest removal was

Table 3
Definitions of error functions and statistical comparison values

Error function	Definition	Remarks	References
ERRSQ	$\sum_{i=1}^p (q_{e,\text{meas}} - q_{e,\text{Calc}})_i^2$	An error function more helpful at the higher end of the liquid phase concentration ranges. The increasing trend in the magnitude and squares of the errors illustrates a better fit for the deviation of models parameters	[28,29,75,76]
HYBRID	$\sum_{i=1}^p \left[\frac{(q_{e,\text{meas}} - q_{e,\text{Calc}})_i^2}{q_{e,\text{meas}}} \right]_i$	It was introduced to improve the fit of ERRSQ method at low concentration ranges	[28,29,75,76]
MPSD	$\sum_{i=1}^p \left(\frac{q_{e,\text{meas}} - q_{e,\text{Calc}}}{q_{e,\text{meas}}} \right)_i^2$	This function is similar to geometric error distribution which was modified to allow for the number of degrees of freedom of the system	[28,29,75,76]
ARE	$\sum_{i=1}^p \left \frac{q_{e,\text{meas}} - q_{e,\text{Calc}}}{q_{e,\text{meas}}} \right _i$	It shows a under or overestimates the experimental data and attempts to minimize the fractional error distribution across the entire limits of the concentration	[28,29,75,76]
EABS	$\sum_{i=1}^p q_{e,\text{meas}} - q_{e,\text{Calc}} _i$	A function similar to ERRSQ function, with an increase in the errors will provide a better fit, leading to the bias towards the higher concentration data	[28,29,75,76]
Sum of normalized errors	–	–	[28,29,66]
Coefficient of determination (R^2)	$\frac{(q_{e,\text{meas}} - q_{e,\text{calc}})^2}{\sum_{i=1}^p (q_{e,\text{meas}} - q_{e,\text{calc}}) + (q_{e,\text{meas}} - q_{e,\text{calc}})^2}$	It is used to test the best-fitting isotherms. If its value closer to unity the goodness of the model is perfect	[28,29]
RMSE	$\sqrt{\frac{1}{p-2} \sum_{i=1}^p (q_{e,\text{meas}} - q_{e,\text{Calc}})^2}$	An estimator used to quantify the difference between values implied by calculated and the measured values of the quantity being estimated	[28,29]
Non-linear chi-square test (χ^2)	$\sum_{i=1}^p \left(\frac{q_{e,\text{meas}} - q_{e,\text{Calc}}}{q_{e,\text{meas}}} \right)_i^2$	A statistical tool necessary for the best fit of an adsorption system. Small value indicates its similarities while a larger number represents the variation of the experimental data	[28,29]

observed at basic pH of 12. The mechanism of pH dependence of BR9 removal may be explained by the nature of dye binding active sites and the chemistry of the BR9 in the solution [8,9,80]. When pH increased from 2 to 12, the negative charge density on the ICSAC surface may get increased due to the reduction of hydrogen ions concentration on the sorption sites. Due to which electrostatic attraction of the BR9 cations was facilitated and the percentage of removal was increased from 69.52 to 92.12%. Instead at low pH, the competition between hydrogen and BR9 cations on the sorption sites possibly resulted due to the high density of hydrogen ions leading to high electrostatic repulsion which did not favour the dye cationic adsorption. Similar results were also reported in literatures for different biomass systems [8,81–83].

3.2. Effect of temperature

The effect of aqueous phase temperature on the adsorption of BR9 was investigated at three different temperatures keeping all other experimental conditions constant as mentioned in Table 2. Increase in operating temperature from 20 to 40°C depicted a noticeable improvement in percentage dye removal from 74.96 to 88.25%. The percentage BR9 removal increased with increasing temperature; illustrating that the enthalpy change had positive values and the adsorption process was endothermic (Fig. 3). The raise in solution temperature (20–40°C) increased the surface activity and kinetic energy of the BR9 molecules which in turn increase film mass transfer across the liquid surrounding the ICSAC particles. In other view, the increase in the rate of diffusion of BR9 molecules

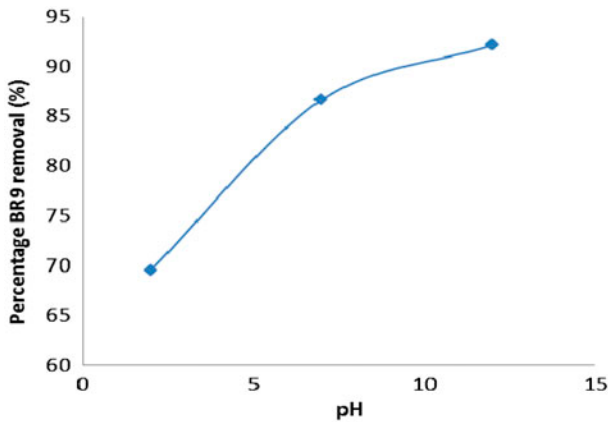


Fig. 2. Effect of initial pH on the removal of BR9 by ICSAC (Contact time: 3h, initial dye concentration: 150 mg/l, temperature: 30°C and adsorbent dose: 5 mg/l).

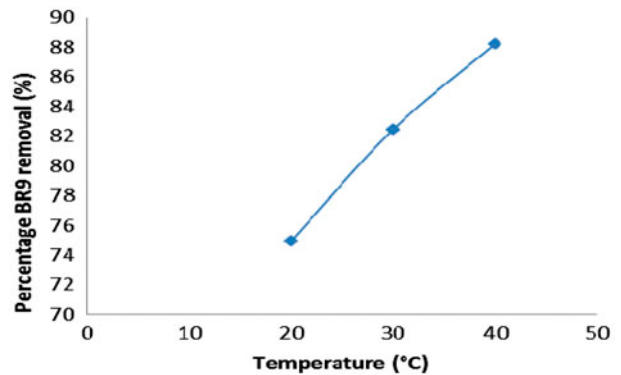


Fig. 3. Effect of temperature on the removal of BR9 by ICSAC (Contact time: 3h, initial dye concentration: 150 mg/l, adsorbent dose: 5 mg/l and initial pH: 12).

at higher temperature across the boundary layer and into the pores might be owing to the decrease in viscosity of solution which could be the cause for the increase in percentage removal of BR9 [8,9,80].

3.3. Effect of contact time and initial dye concentration

In order to find equilibrium time, the sorption of BR9 onto ICSAC was observed as a function of time at optimum pH and temperature (pH: 12 and 40°C) until the amount of BR9 sorbed became constant. The influence of contact time on percentage BR9 removal with respect to dye concentration was shown in Fig. 4. Initially, high uptake of the dye was observed as 86.32, 79.46, 78.47, 74.87 and 71.63% at relatively less contact time of 30 min for 50, 100, 150, 200 and

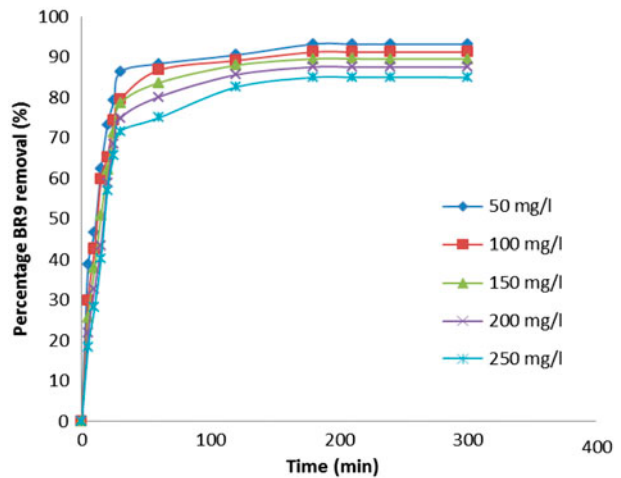


Fig. 4. Effect of initial dye concentration and contact time on the removal of BR9 by ICSAC (Temperature: 40°C, pH: 12, contact time: 5 h and adsorbent dose: 5 mg/l).

Table 4
Sample calculation for SNE

S. no.	Steps to calculate SNE	Sample calculation
1	Selecting an error function at a time and determining the isotherm parameters in order to minimize that error function to produce the isotherm parameter set for that error function	Error function selected: ERRSQ Isotherm selected: Langmuir
2	Determining the error values for all the other error functions for that isotherm parameter set	Evaluate HYBRID (0.082040), MPSD (0.608274), ARE (0.128657), and EABS (1.719076) error values
3	Calculating all other parameter sets for each error function and all their related error functions	Similarly repeat step 1 and 2 for HYBRID, MPSD, ARE, and EABS error functions
4	Selecting each error function in turn and ratio the errors determined for a given parameter set by the maximum for that error function to get the normalized errors	Ratio obtained for ERRSQ: 2.317864 Normalised errors calculated: 0.394525, 0.8058939, 0.776304, 0.982974, 0.594679
5	Summing all these normalized errors for each parameter set	SNE calculated for ERRSQ: 3.554375 Similarly obtain SNE for HYBRID, MPSD, ARE, and EABS error functions

Table 5
Error functions and sum of normalised errors for one and two-parameter models

S.no.	Models	ERRSQ	HYBRID	MPSD	ARE	EABS	SNE
<i>One-parameter models</i>							
1.	Henry						
	ERRSQ	160.653516	7.857224	0.502899	2.234952	27.213862	2.231175
	HYBRID	174.285471	7.479660	0.449101	1.946615	26.062516	2.030498
	MPSD	270.925281	8.763720	0.410076	1.639090	29.560050	2.006052
	ARE	1594.739544	39.831984	1.040582	1.276132	60.490129	4.570989
	EABS	185.801154	7.528109	0.435412	1.850905	25.650083	1.976138
<i>Two-parameter models</i>							
2.	Langmuir						
	ERRSQ	0.914454	0.082040	0.008274	0.128657	1.719076	3.554375
	HYBRID	1.175128	0.069034	0.005483	0.130374	2.276283	3.483062
	MPSD	2.317864	0.087760	0.004394	0.130886	2.890765	4.274381
	ARE	1.087073	0.075248	0.006912	0.125847	1.909798	3.478883
	EABS	1.023004	0.101800	0.010658	0.130611	1.438052	3.936719
3.	Freundlich						
	ERRSQ	4.121369	0.234662	0.019034	0.208475	4.186163	4.215528
	HYBRID	5.002518	0.183844	0.009578	0.191427	4.547969	3.614910
	MPSD	7.339624	0.216429	0.007545	0.183974	5.002815	3.957924
	ARE	8.685112	0.259515	0.011590	0.162721	4.204332	4.229800
	EABS	4.468958	0.234708	0.017459	0.201657	4.075825	4.118211
4.	Temkin						
	ERRSQ	15.064704	0.867680	0.064563	0.479919	7.791384	3.302019
	HYBRID	17.789569	0.707498	0.035548	0.370673	8.401969	2.957623
	MPSD	25.950960	0.812035	0.030251	0.340972	9.278272	3.358688
	ARE	20.341308	0.884838	0.041959	0.281857	7.643422	3.027508
	EABS	16.935799	1.329384	0.124581	0.675147	7.758856	4.488847
5.	Dubinin–Radushkevich						
	ERRSQ	30.704006	2.242185	0.207124	1.003498	10.950440	3.503914
	HYBRID	40.566571	1.664904	0.094987	0.642040	12.602772	2.883082
	MPSD	66.489856	2.012187	0.073526	0.567436	14.844636	3.410275
	ARE	58.341384	2.301585	0.101790	0.452379	13.143332	3.279727
	EABS	34.378510	2.876370	0.287608	1.246920	9.175997	4.135184
6.	Smith						
	ERRSQ	28.335324	1.631319	0.131992	0.523886	11.134299	3.541816
	HYBRID	33.929517	1.274628	0.064948	0.526905	12.209165	3.330747
	MPSD	47.832146	1.464196	0.052972	0.489995	12.705107	3.589064
	ARE	52.254243	1.610039	0.072213	0.449884	11.653201	3.649906
	EABS	37.509469	2.675886	0.243769	0.538927	10.418795	4.537874
7.	Jovanovic						
	ERRSQ	2.699841	0.219652	0.021452	0.226274	3.156866	3.270029
	HYBRID	3.434938	0.185700	0.014507	0.215140	3.896191	3.145411
	MPSD	6.762387	0.239644	0.011543	0.225317	5.160696	4.000338
	ARE	3.390356	0.201032	0.017375	0.205255	3.333676	3.135012
	EABS	3.374575	0.307786	0.030960	0.265419	3.067218	4.093363

250 mg/l, respectively. This rapid adsorption uptake of BR9 enumerated the chemisorption nature of sorption onto ICSAC [84,85]. After 180 min, there was only

a slight difference in the percentage BR9 removal, hence the equilibrium time is considered as 180 min independent of the initial dye concentrations. It was

Table 6
Error functions and sum of normalized errors for three-parameter models

S.no.	Models	ERRSQ	HYBRID	MPSD	ARE	EABS	SNE
1.	Redlich–Peterson						
	ERRSQ	0.195772	0.011966	0.000911	0.050060	0.850113	2.564879
	HYBRID	0.232039	0.009684	0.000493	0.043992	0.987417	2.193230
	MPSD	0.325682	0.010954	0.000420	0.042977	1.156636	2.333070
	ARE	0.268693	0.012154	0.000598	0.033777	0.845426	2.101303
	EABS	1.227380	0.039305	0.001296	0.057513	1.611584	5.000000
2.	Sips						
	ERRSQ	0.091731	0.005310	0.000381	0.033690	0.600532	4.315560
	HYBRID	0.106123	0.004411	0.000220	0.029695	0.676068	3.816961
	MPSD	0.144903	0.004934	0.000191	0.028949	0.777276	4.206216
	ARE	0.134912	0.005836	0.000282	0.023321	0.595739	4.129877
	EABS	0.107402	0.005412	0.000301	0.026826	0.511378	3.913050
3.	Toth						
	ERRSQ	11.775737	160.653516	7.857233	0.502900	2.234956	0.705476
	HYBRID	174.284326	7.479660	0.449103	1.946627	26.062564	2.953981
	MPSD	5.811680	270.924242	8.763701	0.410076	1.639092	0.694733
	ARE	7.186568	1594.736473	39.831908	1.040580	1.276132	2.622198
	EABS	185.801134	7.528109	0.435412	1.850906	25.650083	2.950652
4.	Hill						
	ERRSQ	0.091729	0.005292	0.000378	0.033640	0.601156	3.694695
	HYBRID	0.106182	0.004411	0.000220	0.029685	0.676203	3.393508
	MPSD	0.144896	0.004934	0.000191	0.028947	0.777241	3.795558
	ARE	0.136047	0.005853	0.000282	0.023352	0.598045	3.634558
	EABS	0.102063	0.007132	0.000593	0.037023	0.547546	4.408860
5.	Khan						
	ERRSQ	0.268333	0.017144	0.001358	0.060131	0.990693	3.877436
	HYBRID	0.323601	0.013669	0.000709	0.052225	1.157172	3.303112
	MPSD	0.463718	0.015585	0.000598	0.051193	1.376572	3.654440
	ARE	0.379226	0.015600	0.000757	0.047216	1.108629	3.395921
	EABS	0.661867	0.021496	0.000737	0.050852	1.468822	4.388670
6.	BET						
	ERRSQ	0.382582	0.028526	0.002532	0.079410	1.202357	3.685350
	HYBRID	0.468741	0.023125	0.001438	0.067279	1.298321	3.097122
	MPSD	0.723000	0.027032	0.001191	0.067831	1.652945	3.511764
	ARE	0.752344	0.036813	0.001883	0.058850	1.349709	3.756854
	EABS	1.216823	0.041759	0.001562	0.066300	1.748018	4.451863
7.	Vieth–Sladek						
	ERRSQ	0.190172	0.007298	0.000394	0.034662	0.819208	4.347199
	HYBRID	0.193252	0.007203	0.000385	0.034239	0.821127	4.318607
	MPSD	0.201948	0.007287	0.000382	0.034019	0.829103	4.356934
	ARE	0.230853	0.008332	0.000417	0.031313	0.699977	4.418299
	EABS	0.272558	0.009418	0.000444	0.029638	0.662461	4.654086
8.	Radke–Prausnitz						
	ERRSQ	0.385827	0.013145	0.000572	0.041383	1.131012	4.546006
	HYBRID	0.386056	0.013137	0.000571	0.041532	1.130185	4.547254
	MPSD	0.387686	0.013161	0.000570	0.041112	1.114005	4.526616
	ARE	0.477572	0.015475	0.000625	0.036593	0.955883	4.698403
	EABS	0.483994	0.015625	0.000628	0.036492	0.953060	4.721302

(Continued)

Table 6 (Continued)

S.no.	Models	ERRSQ	HYBRID	MPSD	ARE	EABS	SNE
9.	Brouers–Sotolongo						
	ERRSQ	0.190187	0.002342	0.021392	0.002248	0.000239	3.107889
	HYBRID	0.021414	0.002246	0.000239	0.017671	0.189853	2.723091
	MPSD	0.025009	0.002358	0.000243	0.019699	0.253209	3.142863
	ARE	0.021872	0.002263	0.000240	0.017669	0.192216	2.741789
	EABS	0.022485	0.002272	0.000240	0.017697	0.199869	2.780747
10.	Fritz–Schluender-III						
	ERRSQ	0.195772	0.011958	0.000910	0.050039	0.850108	4.310076
	HYBRID	0.232166	0.009684	0.000493	0.043984	0.987686	3.775141
	MPSD	0.326197	0.010964	0.000420	0.042981	1.157394	4.214847
	ARE	0.265513	0.012260	0.000609	0.033366	0.817039	3.856054
	EABS	0.208151	0.012216	0.000882	0.047786	0.780080	4.232784
11.	Unilin						
	ERRSQ	0.023153	0.002311	0.000242	0.020130	0.232688	4.915486
	HYBRID	0.023229	0.002307	0.000241	0.019908	0.233218	4.905919
	MPSD	0.023254	0.002307	0.000241	0.019784	0.230132	4.887696
	ARE	0.023449	0.002315	0.000242	0.019486	0.225974	4.867677
	EABS	0.024829	0.002344	0.000242	0.019245	0.223574	4.914668

evident from sorption profile that the rate of BR9 removal was rapid initially and became sluggish gradually until the equilibrium time was reached. The percentage BR9 removal was slowly increasing in all the cases (50–250 mg/l) and almost reached steady state values such as 93.21, 91.23, 89.56, 87.54 and 84.97%, respectively. The dye adsorption capacity of ICSAC decreased with the increase of initial dye concentrations certainly due to the unavailability of active sites to dye molecules on ICSAC particles [8,9,80].

3.4. Error analysis

In order to optimize the design of adsorption system for the removal of dyes from aqueous solution, it is important to establish the most appropriate correlation for equilibrium curves. To investigate the suitability of the prevailing isotherm models to describe the adsorption equilibrium, the common approach could be considering the number of parameters in a model. Hence, 24 isotherm models were selected from literature and grouped according to their number of parameters and analysed to understand their suitability for the current adsorption equilibrium data.

On the basis of the sum of normalized errors' procedure as described in Table 4, respective SNE values were determined and displayed in Tables 5–7. Then, the error function which gave minimum SNE value

was selected to calculate the optimum parameter set for that isotherm model. Minimizing the EAB error function was deemed to provide optimum parameters based on the respective SNE value which is comparatively smaller than other error functions for the single-parameter Henry's law. As the two-parameter models were concerned, the HYBRID error function produced the optimum parameter sets based on the lowest SNE for all the models except Langmuir and Jovanovic isotherms. The optimum parameters of Langmuir and Jovanovic isotherms were determined by the ARE error function. Majority of the three-parameter models such as Sips, Hill, Khan, BET, Fritz–Schluender-III Vieth–Sladek and Brouers–Sotolongo isotherms formed optimum parameter sets via minimizing the HYBRID error function. MPSD error function produced optimum parameter sets for Toth and Radke–Prausnitz isotherms. The remaining two isotherms (Redlich–Peterson and Unilin) obtained their optimum parameter sets through minimizing the ARE error function for which the SNE values found to be low. Among the four-parameter models, optimum isotherm sets for Baudu, Marczewski–Jaroniec and Weber–van Vliet isotherms were based on ARE error function, in turn HYBRID created optimum sets for Parker isotherms and MPSD for Fritz–Schluender-IV isotherm. Optimum parameter set for the five-parameter Fritz–Schluender-IV isotherm was determined by the minimization of ARE error function. Table 8 provides the summary of the above discussion.

Table 7
Error functions and sum of normalized errors for four and five-parameter models

S.no.	Models	ERRSQ	HYBRID	MPSD	ARE	EABS	SNE
<i>Four-parameter models</i>							
1.	Baudu						
	ERRSQ	0.024816	0.002363	0.000244	0.021054	0.259451	4.838731
	HYBRID	0.024948	0.002358	0.000243	0.020763	0.259274	4.824446
	MPSD	0.025325	0.002362	0.000243	0.020596	0.261475	4.839311
	ARE	0.025428	0.002374	0.000243	0.020068	0.240309	4.744249
	EABS	0.028148	0.002437	0.000245	0.019754	0.239227	4.853152
2.	Parker						
	ERRSQ	2.694446	0.099291	0.004180	0.128249	3.380969	3.551108
	HYBRID	2.871128	0.093511	0.003462	0.125215	3.465251	3.459249
	MPSD	3.350424	0.098913	0.003258	0.121734	3.547395	3.548730
	ARE	5.347455	0.178966	0.007213	0.122896	3.408474	4.849745
	EABS	4.809381	0.177026	0.007751	0.126888	3.411034	4.839482
3.	Marczewski–Jaroniec						
	ERRSQ	0.023109	0.002306	0.000242	0.019899	0.232071	4.702415
	HYBRID	0.023192	0.002303	0.000241	0.019679	0.232107	4.692306
	MPSD	0.023443	0.002306	0.000241	0.019555	0.234290	4.705486
	ARE	0.023467	0.002312	0.000241	0.019141	0.217747	4.620194
	EABS	0.027293	0.002470	0.000248	0.020604	0.236304	5.000000
4.	Fritz–Schlunder-III						
	ERRSQ	1.712830	0.067039	0.003008	0.106232	2.681811	5.000000
	HYBRID	0.020785	0.002226	0.000239	0.016885	0.157509	0.342354
	MPSD	0.020777	0.002226	0.000239	0.016847	0.156720	0.341682
	ARE	0.020786	0.002226	0.000239	0.016878	0.157061	0.342116
	EABS	0.115520	0.006774	0.000469	0.036549	0.611353	0.896417
5.	Weber–van Vliet						
	ERRSQ	0.612962	0.061094	0.010299	0.165305	1.568018	3.336464
	HYBRID	0.891618	0.050512	0.004573	0.131948	1.822823	2.832961
	MPSD	1.767580	0.066690	0.003330	0.121848	2.416944	3.578525
	ARE	0.817832	0.031805	0.001377	0.101898	1.444704	2.019856
	EABS	1.305156	0.099713	0.011702	0.194906	1.878371	4.515553
<i>Five-parameter model</i>							
1.	Fritz–Schlunder-V						
	ERRSQ	0.020731	0.002224	0.000239	0.016416	0.147689	4.621423
	HYBRID	0.020731	0.002224	0.000239	0.016417	0.147840	4.622261
	MPSD	0.020732	0.002224	0.000239	0.016404	0.147834	4.621544
	ARE	0.020731	0.002224	0.000239	0.016415	0.147544	4.620644
	EABS	0.021674	0.002267	0.000241	0.018125	0.187648	5.000000

It was inferred from Table 8 that the HYBRID error function produced the parameter set in 12 out of 24 selected isotherm models followed by the ARE error function for 9 isotherm models and MPSD error function for two isotherm models. The EAB error function was selected to measure optimum parameter set for only one model.

3.5. Selection of best-fit isotherm

The values of optimum parameter sets calculated based on minimum SNE procedure, coefficient of determination (R^2), RMSE and non-linear chi-square test (χ^2) values were evaluated by considering 95% confidence interval and presented in the Tables 9–11 in order to assess the fitness of the models.

Table 8
Summary on selection of error functions

Isotherm	Error functions based on which optimum set was obtained				
	ERRSQ	HYBRID	MPSD	ARE	EABS
Henry					✓
Langmuir				✓	
Freundlich		✓			
Temkin		✓			
Dubinin–Radushkevich		✓			
Smith		✓			
Jovanovic				✓	
Redlich–Peterson				✓	
Sips		✓			
Toth				✓	
Hill		✓			
Khan		✓			
BET		✓			
Vieth and Sladek		✓			
Radke–Prausnitz			✓		
Brouers–Sotolongo		✓			
Fritz–Schluender-III		✓			
Unilin				✓	
Baudu				✓	
Parker		✓			
Marczewski –Jaroniec				✓	
Fritz–Schlunder-IV			✓		
Weber–van Vliet				✓	
Fritz–Schlunder-V				✓	

Table 9
Optimum isotherm parameters and their statistical comparison values for one-parameter and two-parameter models

S.no.	Models	Constants	Values	R^2	RMSE	χ^2
<i>One-parameter model</i>						
1.	Henry	H (l/mg)	1.4051	0.731253	9.638495	10.277042
<i>Two-parameter models</i>						
1.	Langmuir	q_{mL} (mg/g)	68.1685	0.998428	0.737249	0.080485
		b_L (l/mg)	0.0424			
		R_L	0.1678			
2.	Freundlich	K_f (l/g)	4.7155	0.992764	1.581537	0.181761
		n_f	1.6241			
3.	Temkin	a_T (l/g)	0.5637	0.974269	2.982413	0.688203
		b_T (J/mol)	200.6966			
4.	Dubinin–Radushkevich	q_{mDR} (mg/g)	45.6829	0.941324	4.503697	1.278138
		K_{DR}	0.0027			
5.	Smith	W_{s1}	8.4807	0.950924	4.118830	1.122819
		W_{s2}	1.0344			
6.	Jovanovic	q_{mj} (mg/g)	46.9279	0.995096	1.301990	0.142689
		K_j	–0.0561			

Table 10
Optimum isotherm parameters and their statistical comparison values for three-parameter models

S.no.	Models	Constants	Values	R^2	RMSE	χ^2
1.	Redlich–Peterson	K_{RP1} (l/g)	3.8062	0.998225	0.783384	0.040308
		K_{RP2} (l/mg)	0.1542			
		β_{RP}	0.7513			
2.	Sips	q_{mS} (mg/g)	91.5146	0.999850	0.227398	0.004401
		K_S (l/g)	0.0397			
		n_S	1.1744			
3.	Toth	q_{mT} (mg/g)	69.9136	0.998530	0.712782	0.103543
		K_T	24.8254			
		n_T	1.0000			
4.	Hill	q_{mH} (mg/g)	91.5229	0.999846	0.230415	0.093542
		K_H	25.1589			
		n_H	0.8514			
5.	Khan	q_{mK} (mg/g)	25.9281	0.999532	0.402244	0.101342
		a_K	0.6153			
		b_K	0.1309			
6.	BET	q_{mBET} (mg/g)	45.5353	0.999322	0.484118	0.106279
		α_{BET}	0.0707			
		β_{BET}	0.0049			
7.	Vieth–Sladek	q_{mVS} (mg/g)	17.7646	0.999720	0.310847	0.007070
		b_{VS}	0.2307			
		n_{VS}	0.5657			
8.	Radke–Prausnitz	q_{mRP} (mg/g)	803.5459	0.999439	0.440276	0.012702
		K_{RP}	0.2059			
		n_{RP}	0.4829			
9.	Brouers–Sotolongo	q_{mBS} (mg/g)	58.0109	0.999969	0.103475	0.002343
		K_{BS}	0.0585			
		n_{BS}	0.8587			
10.	Fritz–Schluender-III	q_{mFS} (mg/g)	24.9464	0.999664	0.340709	0.009639
		K_{FS}	0.1497			
		n_{FS}	0.7519			
11.	Unilin	q_{mU} (mg/g)	80.7100	0.999966	0.108279	0.002517
		a_U	33.4374			
		b_U	-1.0999			

Henry's law was applied to describe the experimental data obtained for the sorption of BR9 onto IMCSAC (Fig. 5). The poor values of R^2 (0.731253), RMSE (9.638495) and χ^2 (8.262612) indicated that this model utterly failed to predict the equilibrium data (Table 9). Commonly, the equilibrium adsorption data were obtained at higher equilibrium solute concentrations, where the adsorbent surface was almost at the verge of saturation. Therefore, this study proved the failure of Henry's law at the high ranges of residual solute concentration.

Among the two-parameter models, the Langmuir isotherm provided a good fit to the experimental data with high R^2 (0.989940), low RMSE (0.737249) and

good χ^2 (0.071594) values (Table 9). This proved the homogeneous and monolayer mode of adsorption of BR9 onto ICSAC. Additionally, it supported the assumption that adsorption of BR9 occurred uniformly on the active sites of the adsorbent and once a molecule occupies a site, no further adsorption could take place at this site. The separation factor (R_L) value determined from the Langmuir isotherm indicated that dye adsorption onto IMSAC was in favourable region ($R_L < 1$). Comparing the other literatures, the S_{sp} value of the present study (3.73 m²/g) was well within the range (Table 12). On the other hand, the Jovanovic model fits the experimental data fairly with R^2 (0.988624) next to Langmuir isotherm which was

Table 11
Optimum isotherm parameters and their statistical comparison values for four and five-parameter models

S.no.	Models	Constants	Values	R^2	RMSE	χ^2
1.	Baudu	q_{mB} (mg/g)	41.2820	0.9999632	0.1127571	0.0025900
		b_B	0.0705			
		x	-0.0878			
		y	0.1232			
2.	Parker	q_{mP} (mg/g)	144.0384	0.9958471	1.1981503	0.0931399
		b_P	0.8593			
		C_s (mg/l)	207.2999			
		a_P	0.0009			
3.	Marczewski –Jaroniec	q_{mMJ} (mg/g)	62.2060	0.9999661	0.1083218	0.0024984
		K_{MJ}	0.0438			
		n_{MJ}	0.9692			
		m_{MJ}	0.8693			
4.	Fritz–Schlunder-IV	A_{FS}	3.2275	0.9999699	0.1019249	0.0023566
		B_{FS}	0.0248			
		a_{FS}	0.8859			
		b_{FS}	0.9867			
5.	Weber–van Vliet	P_1	8.3114	0.9999695	0.6394654	0.0587727
		P_2	-4.3525			
		P_3	-0.2726			
		P_4	1.9672			
<i>Five-parameter model</i>						
1.	Fritz–Schlunder-V	q_{mFS5} (mg/g)	75.0594	0.9999700	0.1018119	0.0023423
		K_1	0.0436			
		K_2	0.0210			
		α_{FS}	0.8697			
		β_{FS}	0.9941			

inferred from its values of RMSE (1.301990) and χ^2 (0.104817) comparatively yet having lower maximum adsorption capacity (46.9279 mg/g) than Langmuir isotherm. In turn, Freundlich isotherm (Table 9) almost fitted to the equilibrium data supporting the assumptions of heterogeneous mode of adsorption to certain extent. The value of $1/n_F$ (0.6157) of the Freundlich isotherm proved that the adsorption of BR9 onto ICSAC was cooperative adsorption. The Temkin ($R^2 = 0.835366$), the Smith ($R^2 = 0.685999$) and Dubinin–Radushkevich ($R^2 = 0.624576$) isotherms unable to fit the data meant that the adsorption mechanism did not proceed either with progressive enlargement of adsorbent surfaces or heterogeneous manner in total which was visibly known from their poor values of R^2 , RMSE and χ^2 . Fig. 6 collectively represents all the two-parameter isotherm models.

The abilities of the three-parameter equations to model the equilibrium adsorption data were tested using non-linear regression analysis and their isotherm parameters are shown in Table 10. According to the R^2 , RMSE and χ^2 values, the best-fitted adsorption isotherm models were found in the order: Brouers–Sotol-

ongo > Unilin > Sips > Hill > Vieth–Sladek > Fritz–Schlunder-III > Redlich–Peterson > Khan > Radke–Prausnitz > BET. The adequacy of these isotherms further confirmed the homogeneous adsorption on the heterogeneous surface of IMSAC and the cooperative mani-

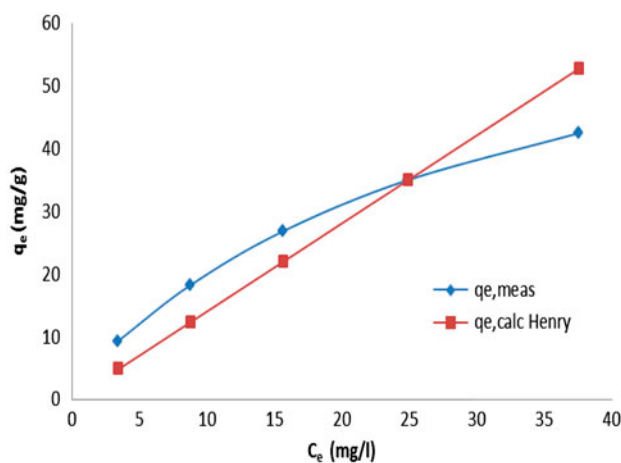


Fig. 5. Comparison of measured and calculated q_e values for single-parameter isotherm.

Table 12
Maximum adsorption capacity and specific surface area values for different adsorbents

S.no.	Adsorbent	q_{\max} (mg/g)	S_{sp} (m ² /g)	Ref.
1.	Bottom ash	6.39	0.34	[82]
2.	Deoiled soya	12.03	0.64	[82]
3.	Jalshakti	11.70	0.63	[86]
4.	Graphene-based magnetic nanocomposite	89.40	4.78	[87]
5.	Sodium sulphite modified cation-exchange resin	127.0	6.79	[88]
6.	Pirina	189.30	10.12	[89]
7.	Cross-linked poly(hydroxyl ethyl methacrylate) resin	134.10	7.17	[90]
8.	AC/ferrospinel composite	101.00	5.40	[91]
9.	Industrial sludges	70.40	3.77	[92]
10.	Methacrylic acid-graft-poly (ethylene terephthalate) fibres	250.00	13.37	[83]
11.	Merck Activated carbon	131.00	7.01	[93]
12.	Cellulose modified with maleic anhydride	31.92	1.71	[94]
13.	Sunflower stalks	187.32	10.02	[95]
14.	Sunflower stalks—chemically treated	204.60	10.94	[95]
15.	Zizania latifolia activated carbon	135.14	7.23	[96]
16.	Fe-modified Zizania latifolia activated carbon	212.77	11.38	[96]
17.	Mn-modified Zizania latifolia activated carbon	238.10	12.73	[96]
18.	Bleaching earth	344.83	18.44	[97]
19.	Tubular structured meso-porous carbon (CMK-5)	1403.00	75.03	[98]
20.	IMCSAC	69.82	3.73	This study

festations of the adsorptive BR9 molecules. The maximum adsorption capacity predicted by the Sips, Hill and Unilin isotherms were higher than Langmuir isotherm but it was found opposite in the case of Khan, BET, Brouers–Sotolongo and Vieth–Sladek isotherms (Table 10). The values of Redlich–Peterson model exponent β_{RP} (0.7513), Sips model exponent n_S (1.1744) and Khan model exponent a_K (0.6153) indicated that

the sorption data were more of a Langmuir form rather than that of Freundlich isotherm. The Hill exponent n_H was less than unity (0.8514), conveyed the idea that the binding interaction between BR9 molecule and IMCSAC was in the form of negative cooperativity. Though the R^2 values were moderately good for all the

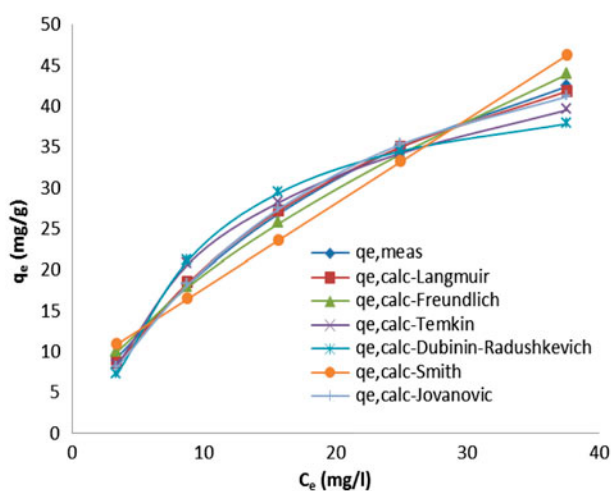


Fig. 6. Comparison of measured and calculated q_e values for two-parameter isotherms.

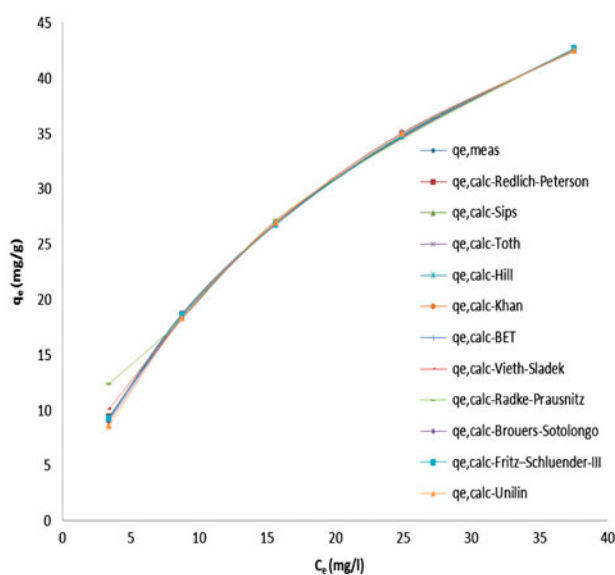


Fig. 7. Comparison of measured and calculated q_e values for three-parameter isotherms.

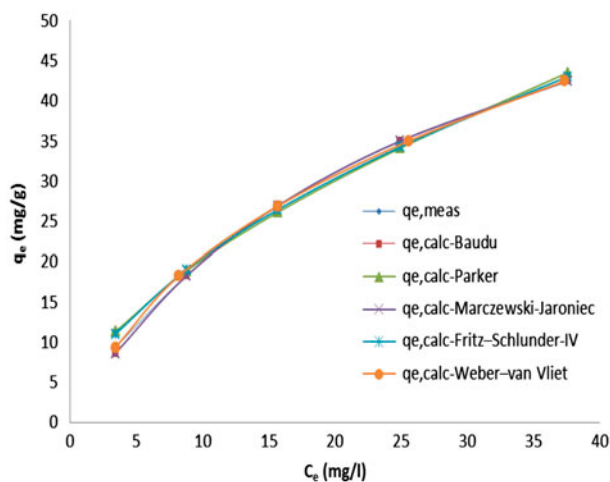


Fig. 8. Comparison of measured and calculated q_e values for four-parameter isotherms.

three-parameter models (Table 10), poor values of the RMSE and χ^2 values clearly indicated that Toth isotherm failed to fit the experimental equilibrium data possibly due to the fact that the majority of the active sites might possess adsorption energy higher than maximum value. Fig. 7 collectively represents all the three-parameter isotherm models.

Among the five isotherms of four-parameter models, very good fitting of the experimental results of adsorption data was obtained using the Fritz–Schlunder-IV isotherm followed by Marczewski–Jaroniec, Baudu, Weber–van Vliet and Parker as mentioned order (Table 11). The Fritz–Schlunder-IV model exponent values a_{FS} (0.8859) and b_{FS} (0.9867) approaching unity indicated that the adsorption data can preferably be fitted with the Langmuir isotherm. An appropriate fitting of the experimental results to Marczewski–Jaroniec, Baudu, Weber–van Vliet and Parker isotherms again affirmed the idea that the adsorption of BR9 onto ICSAC was homogeneous and typically followed Langmuir isotherm nonetheless the adsorption was taking place on the heterogeneous surface (Table 11). Comparison of all four-parameter isotherm models can be made with Fig. 8.

The adsorption data were analysed according to the non-linear form of the five-parameter isotherm model of Fritz–Schlunder-V and a satisfactory fitting of the experimental results was obtained which was known from the comparatively high R^2 (0.9998081), small RMSE (0.1018119) and small χ^2 (0.0023423) values (Table 11). The model exponents of Fritz–Schlunder-V isotherm, α_{FS} (0.8697) and β_{FS} (0.9941) were more close to unity which showed that the adsorption data followed the assumptions of Langmuir isotherm yet the maximum adsorption

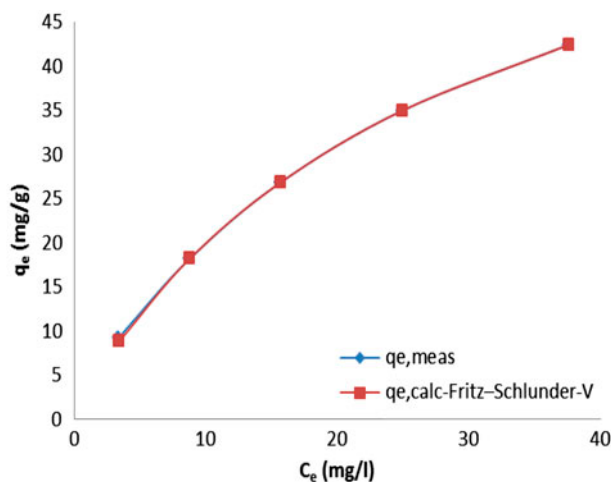


Fig. 9. Comparison of measured and calculated q_e values for five-parameter isotherm.

capacity predicted by this isotherm was greater than Langmuir. Fig. 9 indicates the comparison of calculated q_e with measured q_e for five-parameter isotherm.

By comparing the selected isotherm models, Fritz–Schlunder-V isotherm data having R^2 (0.9998081), RMSE (0.1018119) and χ^2 (0.0023423) were observed as the most valid one for the adsorption equilibrium data. The goodness of the models to explain the equilibrium data was in the order: Fritz–Schlunder-V > Fritz–Schlunder-IV > Brouers–Sotolongo > Unilin > Marczewski–Jaroniec > Baudu > Sips > Hill > Vieth–Sladek Fritz–Schlunder-III > Redlich–Peterson > Khan > Radke–Prausnitz > BET > Weber–van Vliet > Langmuir > Parker > Jovanovic > Freundlich.

4. Conclusions

The activated carbon produced from the immature cotton seeds could be effectively employed for the removal of BR9 from aqueous solution. The batch adsorption studies showed that the equilibrium time for this system would be 180 min. The temperature-dependence study revealed that adsorption of BR9 onto IMSAC was endothermic in nature. The increase in pH proportionate to the percentage removal of BR9 illustrated that adsorption was taking place with ion-exchange. By applying 24 different isotherm models and utilizing the procedure of sum of normalized errors along with the statistical comparison values to obtain optimum parameter sets, the Fritz–Schlunder-V isotherm was found suitable to predict the equilibrium data of adsorption of BR9 onto ICSAC.

Symbols

H	—	Henry constant (l/mg)	b_{VS}	—	Vieth–Sladek equilibrium constant
q_{mL}	—	maximum monolayer adsorption capacity by Langmuir isotherm (mg/g)	n_{VS}	—	Vieth–Sladek model exponent
b_L	—	Langmuir model constant (l/mg)	q_{mRP}	—	maximum monolayer adsorption capacity by Radke–Prausnitz isotherm (mg/g)
R_L	—	separation factor	K_{RP}	—	Radke–Prausnitz equilibrium constant
S_{sp}	—	specific surface area (m ² /g)	n_{RP}	—	Radke–Prausnitz model exponent
K_f	—	Freundlich isotherm constant (l/g)	q_{mBS}	—	maximum monolayer adsorption capacity predicted by Brouers–Sotolongo isotherm (mg/g)
n_f	—	Freundlich exponent	K_{BS}	—	Brouers–Sotolongo equilibrium constant
a_T	—	Temkin isotherm constant (l/g)	n_{BS}	—	Brouers–Sotolongo model exponent
b_T	—	Temkin isotherm constant (J/mol)	q_{mFS}	—	maximum monolayer adsorption capacity predicted by Fritz–Schlunder-III isotherm (mg/g)
q_{mDR}	—	maximum monolayer adsorption capacity by Dubinin–Radushkevich isotherm (mg/g)	K_{FS}	—	Fritz–Schlunder-III equilibrium constant
K_{DR}	—	Dubinin–Radushkevich constant	n_{FS}	—	Fritz–Schlunder-III model exponent
ε	—	Polanyi potential (mol ² /KJ ²)	q_{mU}	—	maximum monolayer adsorption capacity predicted by Unilin isotherm (mg/g)
E	—	mean free energy (kJ/mol)	a_U	—	Unilin equilibrium constant
W_{s1} and W_{s2}	—	Smith isotherm constant	b_U	—	Unilin model exponent
q_{mJ}	—	maximum monolayer adsorption capacity by Jovanovic isotherm (mg/g)	q_{mB}	—	maximum monolayer adsorption capacity predicted by Baudu isotherm (mg/g)
K_J	—	Jovanovic isotherm constant	b_B	—	Baudu equilibrium constant
K_{RP1}	—	Redlich–Peterson isotherm constant (l/g)	x and y	—	Baudu model exponent
K_{RP2}	—	Redlich–Peterson isotherm constant (l/mg)	q_{mP}	—	maximum monolayer adsorption capacity predicted by Parker isotherm (mg/g)
β_{RP}	—	Redlich–Peterson model exponent	b_P	—	Parker equilibrium constant
q_{mS}	—	maximum monolayer adsorption capacity Sips isotherm (mg/g)	C_s	—	concentration required for full surface coverage (mg/l)
K_S	—	Sips model isotherm constant (l/g)	a_P	—	Parker model exponent
n_S	—	Sips model exponent	q_{mMJ}	—	maximum monolayer adsorption capacity by Marczewski–Jaroniec isotherm (mg/g)
q_{mT}	—	maximum monolayer adsorption capacity by Toth isotherm (mg/g)	K_{MJ}	—	Marczewski–Jaroniec equilibrium constant
K_T	—	Toth isotherm constant	n_{MJ} and m_{MJ}	—	Marczewski–Jaroniec model exponent
n_T	—	Toth isotherm exponent	A_{FS} and B_{FS}	—	Fritz–Schlunder-IV equilibrium constant
q_{mH}	—	maximum monolayer adsorption capacity by Hill isotherm (mg/g)	a_{FS} and b_{FS}	—	Fritz–Schlunder-IV model exponent
K_H	—	Hill isotherm Constant	P_1, P_2, P_3 and P_4	—	Weber–van Vliet model parameters
n_H	—	Hill cooperativity coefficient	q_{mFS5}	—	maximum monolayer adsorption capacity by Fritz–Schlunder-V isotherm (mg/g)
q_{mK}	—	maximum monolayer adsorption capacity by Khan isotherm (mg/g)	K_1 and K_2	—	Fritz–Schlunder-V equilibrium constant
a_K	—	Khan isotherm exponent			
b_K	—	Khan isotherm constant			
q_{mBET}	—	maximum monolayer adsorption capacity by BET isotherm (mg/g)			
α_{BET} and β_{BET}	—	BET isotherm constant			
q_{mVS}	—	maximum monolayer adsorption capacity by the Vieth–Sladek isotherm (mg/g)			

α_{FS} and β_{FS}	—	Fritz–Schlunder-V model exponent
$q_{e,meas}$	—	equilibrium adsorption capacity from experiment (mg/g)
$q_{e,calc}$	—	equilibrium adsorption capacity calculated from isotherms (mg/g)
$\overline{q_{e,calc}}$	—	mean equilibrium adsorption capacity calculated from isotherms (mg/g)
n	—	number of data points
p	—	number of variables in the isotherms
χ^2	—	non-linear chi-square test

References

- [1] K.V. Radha, A. Regupathi, T. Arunagiri, T. Murugesan, Decolorization studies of synthetic dyes using *Phanerochaete chrysosporium* and their kinetics, *Process Biochem.* 40 (2005) 3343–3377.
- [2] Y. Fu, T. Viraragvahan, Dye biosorption sites in *Aspergillus niger*, *Bioresour. Technol.* 82 (2002) 139–145.
- [3] G. Bayramoglu, M. Yakup Arica, Biosorption of benzidine based textile dyes “Direct Blue 1 and Direct Red 128” using native and heat-treated biomass of *Trametes versicolor*, *J. Hazard. Mater.* 143 (2007) 135–143.
- [4] F. Roderiguez Reininoso, M. Molino Sabio, Activated carbons from lignocellulosic materials by chemical and/or physical activations: An overview, *Carbon* 30 (1992) 1111–1118.
- [5] S.J.T. Pollard, G.D. Fowler, C.J. Sollars, R. Perry, Low-cost adsorbents for waste and wastewater treatment: A review, *Sci. Total Environ.* 116 (1992) 31–52.
- [6] A. Srinivasan, T. Viraraghavan, Decolorization of dye wastewaters by biosorbents: A review, *J. Environ. Manage.* 91 (2010) 1915–1929.
- [7] S.S. Nawar, H.S. Doma, Removal of dyes from effluents using low-cost agricultural by-products, *Sci. Total Environ.* 79 (1989) 271–279.
- [8] M. Amran, M. Salleh, D.K. Mahmoud, W. Azlina, W.A. Karim, A. Idris, Cationic and anionic dye adsorption by agricultural solid wastes: A comprehensive review, *Desalination* 280 (2011) 1–13.
- [9] M. Rafatullah, O. Sulaiman, R. Hashim, A. Ahmad, Adsorption of methylene blue on low-cost adsorbents: A review, *J. Hazard. Mater.* 177 (2010) 70–80.
- [10] C.A. Philip, Adsorption characteristics of micro porous carbons from apricot stones activated by phosphoric acid, *J. Chem. Tech. Biotechnol.* 67 (1996) 248–254.
- [11] T. Vernersson, P.R. Bonelli, E.G. Cerrella, A.L. Cukierman, *Arundo donax* cane as a precursor for activated carbons preparation by phosphoric acid activation, *Bioresour. Technol.* 83 (2002) 95–104.
- [12] M. Jagtoyen, F. Derbyshire, Activated carbons from yellow poplar and White oak by H_3PO_4 activation, *Carbon* 36 (1998) 1085–1097.
- [13] C. Moreno Castilla, F. Carrasco Marin, M.V. Lopez Ramon, M.A. Alvarez Merino, Chemical and physical activation of olive-mill waste water to produce activated carbons, *Carbon* 39 (2001) 1415–1420.
- [14] J. Hayashi, A. Kazehaya, K. Muroyama, A.P. Watkinson, Preparation of activated carbon from lignin by chemical activation, *Carbon* 38 (2000) 1873–1878.
- [15] C. Namasivayam, D. Sangeetha, Equilibrium and kinetic studies of adsorption of phosphate onto $ZnCl_2$ activated coir pith carbon, *J. Colloid Interface Sci.* 280 (2004) 359–365.
- [16] W.T. Tsai, C.Y. Chang, S.L. Lee, S.Y. Wang, Thermo gravimetric analysis of corn cob impregnated with zinc chloride for preparation of activated carbon, *J. Therm. Anal. Calorim.* 63 (2001) 351–357.
- [17] A.A.M. Daifullah, B.S. Girgis, H.M.H. Gad, A study of the factors affecting the removal of humic acid by activated carbon prepared from biomass material, *Colloids Surf. A* 235 (2004) 1–10.
- [18] K. Jin Wha, S. Myoung Hoi, K. Dong Su, S. Seung Man, K. Young Shik, Production of granular activated carbon from waste walnut shell and its adsorption characteristics for Cu^{2+} ion, *J. Hazard. Mater. B* 85 (2001) 301–315.
- [19] B.S. Girgis, A.E. Abdel Nasser, Porosity development in activated carbons obtained from date pits under chemical activation with phosphoric acid, *Micropor. Mesopor. Mater.* 52 (2002) 105–117.
- [20] Jia Guo, W.S. Xu, Y.L. Chen, A.C. Lua, Adsorption of NH_3 onto activated carbon prepared from palm shells impregnated with H_2SO_4 , *J. Colloid Interface Sci.* 281 (2005) 285–290.
- [21] M.C. Baquero, L. Giraldo, J.C. Moreno, F. Suarez-Garcia, A. Martinez-Alonso, J.M.D. Tascon, Activated carbons by pyrolysis of coffee bean husks in presence of phosphoric acid, *J. Anal. Appl. Pyrolysis* 70 (2003) 779–784.
- [22] Z. Hu, M.P. Srinivasan, Preparation of high surface area activated carbons from coconut shell, *Micropor. Mesopor. Mater.* 27 (1999) 11–18.
- [23] B.S. Girgis, S.S. Yunis, A.M. Soliman, Characteristics of activated carbon from peanut hulls in relation to conditions of preparation, *Mater. Lett.* 57 (2002) 164–172.
- [24] M.J. Martin, A. Artola, M.D. Balaguer, M. Rigola, Activated carbons developed from surplus sewage sludge for the removal of dyes from dilute aqueous solutions, *Chem. Eng. J.* 94 (2003) 231–239.
- [25] <http://www.fas.usda.gov>. Accessed 10 March 2013.
- [26] C. Tien, *Adsorption Calculations and Modeling*, Butterworth-Heinemann Series in Chemical Engineering, Boston, MA, 1994.
- [27] G. McKay, *Use of Adsorbents for the Removal of Pollutants from Wastewaters*, CRC Press, Boca Raton, FL, 1996.
- [28] Y.S. Ho, J.F. Porter, G. McKay, Equilibrium isotherm studies for the sorption of divalent metal ions onto peat: Copper, nickel and lead single component systems, *Water Air Soil Pollut.* 141 (2002) 1–33.
- [29] K.Y. Foo, B.H. Hameed, Insights into the modeling of adsorption isotherm systems, *Chem. Eng. J.* 156 (2010) 2–10.
- [30] J.F. Porter, G. McKay, K.H. Choy, The prediction of sorption from a binary mixture of acidic dyes using single- and mixed-isotherm variants of the ideal adsorbed solute theory, *Chem. Eng. Sci.* 54 (1999) 5863–5885.
- [31] Y.S. Ho, Selection of optimum sorption isotherm, *Carbon* 42 (2004) 2115–2116.
- [32] S.J. Allen, G. McKay, J.F. Porter, Adsorption isotherm models for basic dye adsorption by peat in single and binary component systems, *J. Colloid Interface Sci.* 280 (2004) 322–333.
- [33] Y.C. Wong, Y.S. Szeto, W.H. Cheung, G. McKay, Adsorption of acid dyes on chitosan-equilibrium isotherm analyses, *Proc. Biochem.* 39 (2004) 693–702.
- [34] F.C. Wu, R.L. Tseng, Preparation of highly porous carbon from fir wood by KOH etching and CO_2 gasification for adsorption of dyes and phenols from water, *J. Colloid Interface Sci.* 294 (2006) 21–30.
- [35] Sudhir Dahiya, R.M. Tripathi, A.G. Hegde, Biosorption of lead and copper from aqueous solutions by pre-treated crab and arca shell biomass, *Bioresour. Technol.* 99 (2008) 179–187.
- [36] Sabir Hussain, Hamidi Abdul Aziz, Mohamed Hasnain Isa, M. Nordin Adlan, Faridah, A.H. Asaari, Physico-chemical method for ammonia removal from synthetic wastewater using limestone and GAC in batch and column studies, *Bioreour. Technol.* 98 (2006) 874–880.
- [37] M.R. Othman, A.M. Amin, Comparative analysis on equilibrium sorption of metal ions by biosorbent Tempe, *Biochem. Eng. J.* 16 (2003) 361–364.
- [38] Tamer Akar, Sibel Tunali, Biosorption characteristics of *Aspergillus flavus* biomass for removal of Pb(II) and Cu(II) ions from an aqueous solution, *Bioresour. Technol.* 97 (2006) 1780–1787.

- [39] J.S. Piccin, C.S. Gomes, L.A. Feris, M. Gutterres, Kinetics and isotherms of leather dye adsorption by tannery solid waste, *Chem. Eng. J.* 183 (2012) 30–38.
- [40] F.N. Ridha, P.A. Webley, Anomalous Henry's law behaviour of nitrogen and carbon dioxide adsorption on alkali-exchanged chabazite zeolites, *Sep. Purif. Technol.* 67 (2009) 336–343.
- [41] P. Monash, G. Pugazhenth, Adsorption of crystal violet dye from aqueous solution using mesoporous materials synthesized at room temperature, *Adsorption* 15 (2009) 390–405.
- [42] I. Langmuir, The adsorption of gases on plane surfaces of glass, mica, and platinum, *J. Am. Chem. Soc.* 40 (1918) 1361–1403.
- [43] T.W. Weber, R.K. Chakravorti, Pore and solid diffusion model for fixed bed absorbers, *AIChE J.* 20 (1974) 2228.
- [44] F. Guzel, I. Uzun, Determination of the micropore structures of activated carbons by adsorption of various dyestuffs from aqueous solution, *Turk. J. Chem.* 26 (2002) 369–377.
- [45] C. Kaewprasit, E. Hequet, N. Abidi, J.P. Gourlot, Application of methylene blue adsorption to cotton fiber specific surface area measurement. Part I. Methodology, *J. Cotton Sci.* 2 (1998) 164–173.
- [46] M.I. El Khaiary, Least-squares regression of adsorption equilibrium data: Comparing the options, Least-squares regression of adsorption equilibrium data: Comparing the options, *J. Hazard. Mater.* 158 (2008) 73–87.
- [47] J. Wang, C.P. Huang, H.E. Allen, D.K. Cha, D.W. Kim, Adsorption characteristics of dye onto sludge particulates, *J. Colloid Interface Sci.* 208 (1998) 518–528.
- [48] A.W. Adamson, A.P. Gast, *Physical Chemistry of Surfaces*, 6th ed., Wiley-Interscience, New York, NY, 1997.
- [49] F. Haghseresht, G. Lu, Adsorption characteristics of phenolic compounds onto coal-reject-derived adsorbents, *Energy Fuels* 12 (1998) 1100–1107.
- [50] M.J. Temkin, V. Pyzhev, Kinetics of ammonia synthesis on promoted iron catalysts, *Acta Physicochim. URSS* 12 (1940) 217–222.
- [51] L.V. Radushkevich, Potential theory of sorption and structure of carbons, *Zh. Fiz. Khim.* 23 (1949) 1410–1420.
- [52] M.M. Dubinin, Modern state of the theory of volume filling of micropore adsorbents during adsorption of gases and steams on carbon adsorbents, *Zh. Fiz. Khim.* 39 (1965) 1305–1317.
- [53] S.M. Hasany, M.H. Chaudhary, Sorption potential of Hare River sand for the removal of antimony from acidic aqueous solution, *Appl. Rad. Isot.* 47 (1996) 467–471.
- [54] S.E. Smith, Sorption of water vapour by high polymers, *J. Am. Chem. Soc.* 69 (1947) 646–651.
- [55] D.S. Jovanovic, Physical adsorption of gases. I. Isotherms for monolayer and multilayer adsorption, *Colloid Polym. Sci.* 235 (1969) 1203–1214.
- [56] O. Redlich, D.L. Peterson, A useful adsorption isotherm, *J. Phys. Chem.* 63 (1959) 1024–1026.
- [57] J.C.Y. Ng, W.H. Cheung, G. McKay, Equilibrium studies of the sorption of Cu(II) ions onto chitosan, *J. Colloid Interface Sci.* 255 (2002) 64–74.
- [58] R. Sips, Combined form of Langmuir and Freundlich equations, *J. Chem. Phys.* 16 (1948) 490–495.
- [59] J. Toth, State equations of the solid gas interface layer, *Acta Chem. Acad. Hung.* 69 (1971) 311–317.
- [60] A.V. Hill, The possible effects of the aggregation of the molecules of haemoglobin on its dissociation curves, *J. Physiol.* 40 (1910) 4–7.
- [61] L.K. Koopal, W.H. Van Riemsdijk, J.C.M. de Wit, M.F. Benedetti, Analytical isotherm equation for multicomponent adsorption to heterogeneous surfaces, *J. Colloid Interface Sci.* 166 (1994) 51–60.
- [62] A.R. Khan, R. Ataullah, A. Al Haddad, Equilibrium adsorption studies of some aromatic pollutants from dilute aqueous solutions on activated carbon at different temperatures, *J. Colloid Interface Sci.* 194 (1997) 154–165.
- [63] S. Bruanuer, P.H. Emmett, E. Teller, Adsorption of gases in multi-molecular layers, *J. Am. Chem. Soc.* 60 (1938) 309–316.
- [64] W.R. Vieth, K.J. Sladek, A model for diffusion in a glassy polymer, *J. Colloid Sci.* 20 (1965) 1014–1033.
- [65] C.J. Radke, J.M. Prausnitz, Adsorption of organic solutes from dilute aqueous solutions on activated carbon, *Ind. Eng. Chem. Fundam.* 11 (1972) 445–450.
- [66] S. Kundu, A.K. Gupta, Arsenic adsorption onto iron oxide-coated cement (IOCC): Regression analysis of equilibrium data with several isotherm models and their optimization, *Chem. Eng. J.* 122 (2006) 93–106.
- [67] S.J. Gregg, K.S.W. Sing, *Adsorption, Surface Area and Porosity*, Academic Press, New York, NY, 1967.
- [68] W. Fritz, E.U. Schlunder, Simultaneous adsorption equilibria of organic solutes in dilute aqueous solution on activated carbon, *Chem. Eng. Sci.* 29 (1974) 1279–1282.
- [69] D.P. Valenzuela, A.L. Myers, *Adsorption Equilibria Data Handbook*, Prentice-Hall, Englewood Cliffs, NJ, 1989.
- [70] M. Baudu, Etude des interactions solute-fibres de charbon actif. Application et regeneration, Ph.D. diss., Universite de Rennes I, 1990.
- [71] G.R. Parker, Optimum isotherm equation and thermodynamic interpretation for aqueous 1,1,2-trichloroethene adsorption isotherms on three adsorbents, *Adsorption* 1 (1995) 113–132.
- [72] B.M. van Vliet, W.J. Weber, H. Hozumi, Modelling and prediction of specific compound adsorption by activated carbon and synthetic adsorbents, *Water Res.* 14 (1980) 1719–1817.
- [73] R.H. Myers, Classical and modern regression with applications, PWSKENT 444–445 (1990) 297–298.
- [74] D.A. Ratkowski, *Handbook of Nonlinear Regression Models*, Marcel Dekker, New York, NY, 1990.
- [75] K.V. Kumar, S. Sivanesan, Sorption isotherm for safranin onto rice husk: Comparison of linear and non-linear methods, *Dyes Pigm.* 72 (2007) 130–133.
- [76] Y.S. Ho, Second-order kinetic model for the sorption of cadmium onto tree fern: A comparison of linear and non-linear methods, *Water Res.* 40 (2006) 119–125.
- [77] M.C. Ncibi, Applicability of some statistical tools to predict optimum adsorption isotherm after linear and non-linear regression analysis, *J. Hazard. Mater.* 153 (2008) 207–212.
- [78] T.F. Edgar, D.M. Himmelblau, *Optimization of Chemical Processes*, McGraw-Hill, New York, NY, 1989.
- [79] O.T. Hanna, O.C. Sandall, *Computational Methods in Chemical Engineering*, Prentice-Hall International, Upper Saddle River, NJ, 1995.
- [80] A. Srinivasan, T. Viraraghavan, Decolorization of dye wastewaters by biosorbents: A review, *J. Environ Manage.* 91 (2010) 1915–1929.
- [81] V.K. Gupta, Suhas, Application of low-cost adsorbents for dye removal—A review, *J. Environ Manage.* 90 (2009) 2313–2342.
- [82] V.K. Gupta, A. Mittal, V. Gajbe, J. Mittal, Adsorption of basic fuchsin using waste materials-bottom ash and deoiled soya-as adsorbents, *J. Colloid Interface Sci.* 319 (2008) 30–39.
- [83] M. Arslan, M. Yigitoglu, Use of methacrylic acid grafted poly(ethylene terephthalate) fibers for the removal of basic dyes from aqueous solutions, *J. Appl. Polym. Sci.* 110 (2008) 30–38.
- [84] O. Gulnaz, A. Kaya, F. Matyar, B. Arikan, Sorption of basic dyes from aqueous solution by activated sludge, *J. Hazard. Mater. B* 108 (2004) 183–188.
- [85] J.Y. Farah, N.S. El Gendy, L.A. Farahat, Biosorption of Astrazone Blue basic dye from an aqueous solution using dried biomass of Baker's yeast, *J. Hazard. Mater.* 148 (2007) 402–408.
- [86] R. Dhodapkar, N.N. Rao, S.P. Pande, T. Nandy, S. Devotta, Adsorption of cationic dyes on Jalshakti[®], super absorbent polymer and photocatalytic regeneration of the adsorbent, *React. Funct. Polym.* 67 (2007) 540–548.

- [87] C. Wang, C. Feng, Y. Gao, X. Ma, Q. Wu, Z. Wang, Preparation of a graphene-based magnetic nanocomposite for the removal of an organic dye from aqueous solution, *Chem. Eng. J.* 173 (2011) 92–97.
- [88] G. Bayramoglu, B. Altintas, M.Y. Arica, Adsorption kinetics and thermodynamic parameters of cationic dyes from aqueous solutions by using a new strong cation-exchange resin, *Chem. Eng. J.* 152 (2009) 339–346.
- [89] N. Mehmet, G. Ismail, A. Bilal, Use of pirina pretreated with hydrochloric acid for the adsorption of methyl violet from aqueous solution, *Asian J. Chem.* 24 (2012) 1698.
- [90] G. Bayramoglu, B. Altintas, M. Yakup Arica, Adsorption kinetics and thermodynamic parameters of cationic dyes from aqueous solutions by using a new strong cation-exchange resin, *Chem. Eng. J.* 152 (2009) 339–346.
- [91] L. Ai, J. Jiang, Fast removal of organic dyes from aqueous solutions by AC/ferrospinel composite, *Desalination* 262 (2010) 134–140.
- [92] M. Seredych, T.J. Bandoz, Removal of cationic and ionic dyes on industrial municipal sludge based composite adsorbents, *Ind. Eng. Chem. Res.* 46 (2007) 1786–1793.
- [93] K. Vasanth Kumar, S. Sivanesan, Isotherm parameters for basic dyes onto activated carbon: Comparison of linear and non-linear method, *J. Hazard. Mater. B* 129 (2006) 147–150.
- [94] Y. Zhou, Q. Zhang, Q. Jin, T. Ma, X. Hu, Heavy metal ions and organic dyes removal from water by cellulose modified with maleic anhydride, *J. Mater. Sci.* 47 (2012) 5019–5029.
- [95] W. Shi, X. Xu, G. Sun, Chemically modified sunflower stalks as adsorbents for colour removal from textile wastewater, *J. Appl. Polym. Sci.* 71 (1999) 1841–1850.
- [96] L. Huang, J. Kong, W. Wang, C. Zhang, S. Niu, B. Gao, Study on Fe(III) and Mn(II) modified activated carbons derived from *Zizania latifolia* to removal basic fuchsin, *Desalination* 286 (2012) 268–276.
- [97] W.T. Tsai, Y.M. Chang, C.W. Lai, C.C. Lo, Adsorption of basic dyes in aqueous solution by clay adsorbent from regenerated bleaching earth, *Appl. Clay Sci.* 29 (2005) 149–154.
- [98] G.P. Hao, W.C. Li, S. Wang, S. Zhang, A.H. Lu, Tubular structured ordered mesoporous carbon as an efficient sorbent for the removal of dyes from aqueous solutions, *Carbon* 48 (2010) 3330–3339.